Morphological and Electrical Properties of gold nanoparticles /macroPorous Silicon for CO₂ Gas

Alwan M. Alwan[1], Rasha B. Rashid[*1], Amer B. Dheyab[2]

[1]School of Applied Science, University of Technology, Baghdad,Iraq.
[2]Ministry of Science and Technology, Baghdad, Iraq.

Abstract

In this work, the fine structure macro-porous silicon (macroPS) substrate was prepared by photo-electro-chemical etching of n-type silicon wafer. Ultraviolet illumination condition of wavelength 360nm wavelength and intensity of about $100mW/cm^2$ with etching current density of about $50\ mA/cm^2$ and etching time 5 min was employed. The Hybrid device gold nanoparticles /macroPorous Silicon (AuNPs/macroPS) was fabricated by deposition AuNPs into mPS substrate Via immersion plating process of macroPS in the solution of HAuCl4 with the ($10^{-3}M$) concentration and 2min immersion time. The characteristics of PS before and after immersion process were investigated by scanning electron microscopy (SEM), EDS, X-Ray diffraction (XRD), photoluminescence (PL) and Infrared spectroscopy (FTIR). The J-V characteristics of sandwich structure showed that the maximum sensitivity of the AuNPs/macro PS was about (90.5%)for compared with macro-PS substrate. The current-voltage characteristics were performed in primary vacuum with a base pressure of about 0.2mbar and CO2 with 1mbare concentrations. Significant enhancement was observed in sensitivity of the AuNPs/macroPS hybrid device and temporal response after deposition the AuNPs.

Keywords: Morphological, Gold Nanoparticle, macroPS, Photoluminescence.

<div dir="rtl">

الخصائص المورفولوجية والكهربائية للجسيمات الذهب النانوية مع السيليكون مسامي ماكروية الهجينه مستخدمة في تحسس عن الغازCO₂

علوان محمد علوان¹، رشا بشار رشيد*¹، عامر بدر ذياب²

¹قسم العلوم التطبيقية ، الجامعة التكنولوجية ، بغداد، العراق.
²وزارة العلوم والتكنولوجيا، بغداد، العراق.

الخلاصة

في هذا العمل تم تحضير سيلكون مسامي ماكروي بطريقة التنميش الضوء– كهروكيميائية للشريحة السليكون من النوع المانح. المحضرة باستخدام الليزر البنفسجي ذو الطول الموجي 630 نانومتر ،بشدة اضاءة حوالي 100 ملي واطاسم²،وكثافة تيار التنميش50ملي أمبير/اسم² وزمن التنميش 5 دقائق تم استخدامها خلال عملية التنميش. تم تركيب السليكون المسامي المجرد(قبل عملية الترسيب المعدني) والسليكون المسامي المطعم بجسيمات الذهب النانوية تم دراستها بواسطة قياس حيود الاشعة السينية،المجهر الماسح الالكتروني،وقياس تشتت طاقة الاشعة السينية ، وقياسات التلؤلؤ الضوئي تم دراسته كدالة لحجم جسيمات

</div>

_____
*Email: rasha198585@yahoo.com

الذهب النانوية وتوزيعها على سطح السليكون المسامي، وقياسات تحويلات فورير للاشعة تحت الحمراء وتم دراسة خصائص التيار– فولتية للتركيب الهندسي المركب اظهرت اعلى قيمة للتحسسية لطبقة السليكون المسامي ماكروي مع جسيمات الذهب النانوية حوالي(90.5%) بمقارنه مع العينة السليكون المسامي. وتم قياس خصائص الكهربائية تحت ضغط 0.2 ملي بار، وبعد ذلك مع الغاز تحت تركيز 1بار . ولوحظ تحسن كبير في حساسية للعينة الهجينة والاستجابة الزمنية بعد ترسب جسيمات الذهب النانوية.

1. Introduction

At present Silicon is the main material of micro-electronics; however it is not commonly used in opto-electronics. The reason is owing to the inherent nature of the indirect transition in the band-edge emission. When the visible photoluminescence (PL) of electrochemically etched porous silicon (PS) was reported by Canham in 1990, the material has been extensively studied to explain luminescence mechanism and to investigate its possible use as a new material for the optical device application [1]. The current devices have been proved not only to be individually low-cost and low-power devices, owing to the formation of electroless deposited low resistance [2, 3]. A version process for coating the devices by the electroless deposition of metals provided enhanced sensitivity and selectivity to NO_x, CO, and NH3. The carbon monoxide (CO_2) is normally classified as inert gas inters of an acid-base reaction. The output signal from the untreated porous silicon sensor is a weak signal. The surface treatment of porous silicon with TiO_2 and SnO_2 will improve the output signal from the sensor and hence enhancing the sensing capabilities [4-6], There are several axes for scientific research and applications within the following chemical sensor [7-9], tissue engineering [10], cell culture [11], drug delivery [12], biotechnology, gas separation and microelectronics[13]. Series applications of PS in sensor technology have been based on the change of conductivity or capacity of a material upon adsorption of gas molecules [14]. The gas detection can be carried out to a wide range of physical, chemical, electrochemical and optical principles [15]. Advantages of PS sensors are low cost, room temperature operation and possible integration with electronic circuits [16]. The electrical behavior and sensing properties in exposing to the CO_2 gas of gold electrode on the PS surface have been investigating. The fabrication of hybrid gold nanoparticles on meso-porous silicon (AuNPs/ mesoPS) structures as CO2 gas sensors working at room temperature[17]. In this paper, we the concentrate on study behavior morphological and electrical properties of incorporation gold nanoparticles on macroPorous silicon (AuNPs/ macroPS) for CO2 sensing applications.

2. Experimental

The macroPS samples prepared by photoelectrochemical etching by etching of n-type silicon wafer of (100) orientation and (1-10Ω.cm) resistivity. laser of wavelength (630) nm and fixed output power density of about (100 mW/cm2) was the illumination source employed in this study. In PECE process, Si represents the anode and the platinum ring represents the cathode. The etching time is (5min) and the illuminated area is about (1.5cm^2).Figure-1 below shows the schematic diagram of PECE process. The anodization electrolytes consisted of an alcoholic 48wt% hydrofluoric acid mixture; at a ratio (1:1) in volume, with the following alcohols: 99.8% ethanol (C_2H_5OH), 99.8% methanol.
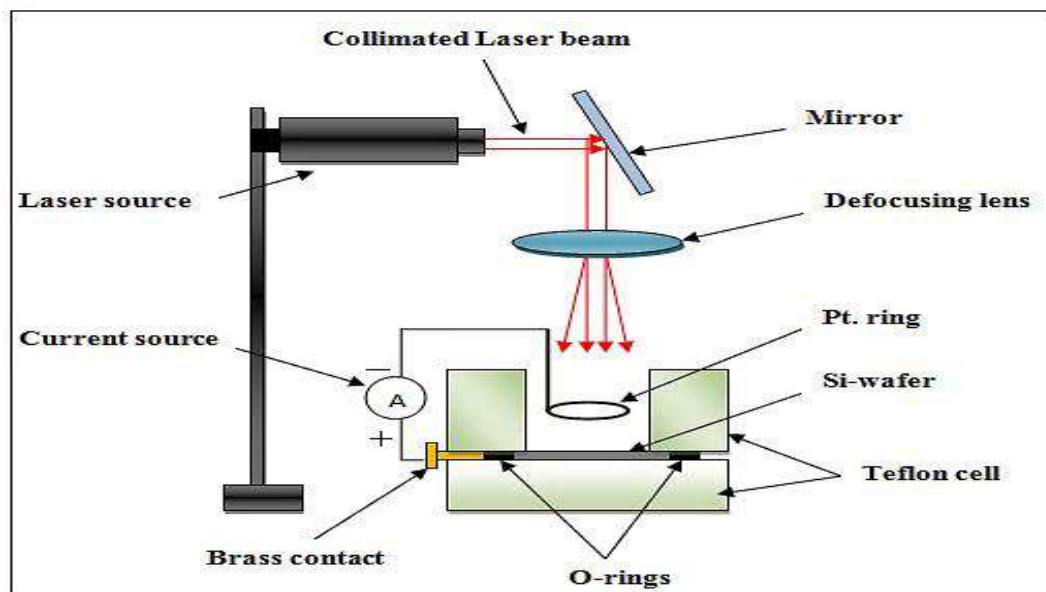
Figure 1- Schematic diagram of photo-electrochemical etching process [18].

The anodized wafer and platinum (pt) cathode were saved parallel to each other with a distance of 1.2 cm between them in the photo-electrochemical cell to formula homogeneity porous Si layers. The current was flowing to the polished surface of the wafer. The etching was done at room temperature. The current density (J) were (50) mA/cm^2 with an etching time 5 min.

The surface morphology of AuNPs/macroPS was observed through (Field Emission SEM AIS3200C) made in the USA. The (PL) data could be read directly from a computer monitor .From the PL curve, the band gap of PS can be determined from the relation [19].

$Eg_{(PS)} = h\,c/\lambda_{max}$ ………………………………………...………(1)

Where h is Planck constant, c is the light speed, and λ_{max} is obtained from the PL curve and then can determine the nano size L according to the following equation

$Eg_{(PS)} = Eg_{(Si)} + 88.34/L^{1.37}$ ………………………………………………………………..(2)

The PL measurement for this work was done by using LiCuix3205N.

This device was made in sandwich form. The device by two Aluminum electrodes was deposited under and top of the device. If a sensor is placed directly in the path of a flow of gas, and as close as possible to the flow as in Figure-2, there exists a flow rate which, when exceeded, leads to an extremely noisy response. This variation is connected to adsorption of the CO_2 molecule on the surface of the gold nanoparticles /macro-porous silicon. layer owing to the Vander Waals interaction. The measurements the forward current-voltage (J–V) characteristics of Al/Au-NPs/n-PSi/Al structures and without coated Al/PS/Al at room temperature. The current passing in the Al/AuNPs/PS/n-Si/Al structures was valied according to the morphologies of the PS substrate and the morphology of the AuNPs layer.
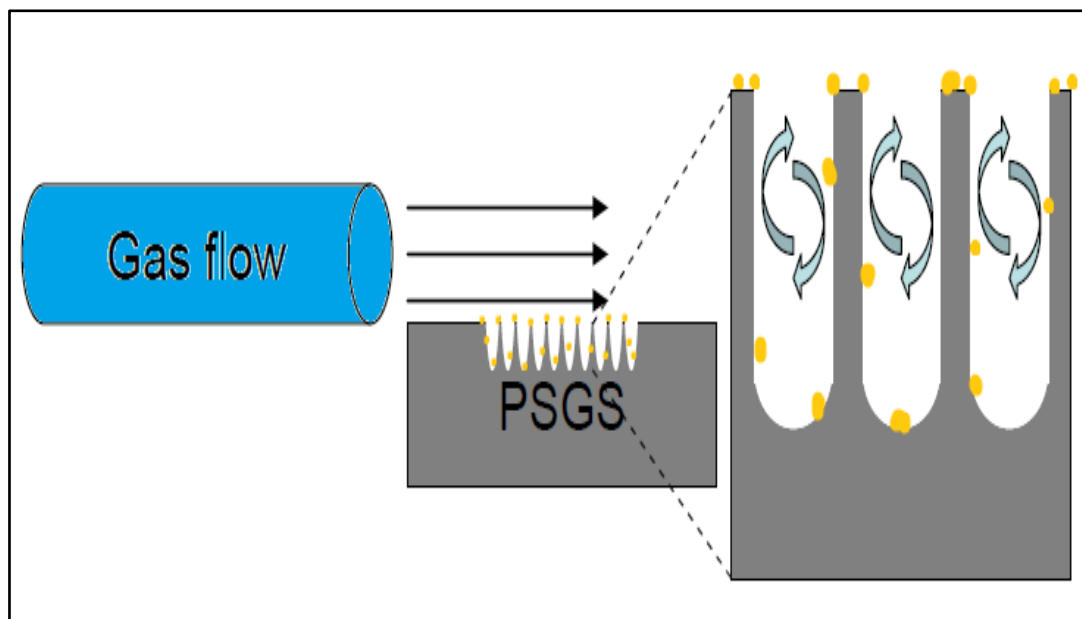
Figure 2-Schematic diagram the flow of gas over the gold nanoparticles / porous silicon surface

The one-dimensional diffusion equation (Equation 3) governs the behavior of the analyte gas within this column[20,21]. The concentration of the analyte gas at one end of the well is provided as an initial condition which can be changed (programmed) between executions of the model. This concentration is given as the variable C_0 represented in Equation 4. A second boundary condition exists at the other end of the well (Equation 5) which provides for no leakage of the analyte through this region3.

$$\frac{\partial C(x,t)}{\partial t} = D\frac{\partial^2 C(x,t)}{\partial x^2} \quad \cdots\cdots\cdots\cdots \quad (3)$$

Where equation 3: The diffusion equation models the diffusion of an analyte concentration 'C' in one dimension. This equation is valid from 0 to the pore length 'L' in 'x' and from 0 to infinity in time 't'. The diffusion constant 'D' governs the rate of diffusion.

$$C(x,t)\Big|_{x=0} = C_0(t) \quad \cdots\cdots\cdots\cdots\cdots \quad (4)$$

Where equation 4: The first boundary condition for the diffusion equation (Equation 3) controls the presence of the analyte at the open end (top) of the pore for all times 't'.

$$\frac{\partial C(x,t)}{\partial x}\bigg|_{x=L} = 0 \quad \cdots\cdots\cdots\cdots \quad (5)$$

Where equation 5: The second boundary condition for the diffusion equation (Equation 3) provides for a zero flux of gas concentration 'C' through the bottom of the pore being modeled.
Finally, the initial conditions for the problem are chosen to represent an 'empty' pore, containing a zero analyte concentration. This is represented as:

$$C(x,t)\Big|_{t=0} = 0 \quad \cdots\cdots\cdots\cdots\cdots \quad (6)$$

Where equation6: The initial condition for pore modeling.
3. Results and Discussion
3.1. Structural Measurement
The surface topographical of AuNPs/PS was carried out by FE-SEM A technique where is shown in Figure-3. The SEM images of pore sizes showed that its shape was mostly different pore sizes with ranging from 2.034 µm to 7.608µm and peak of particle diameter distribution was about 3.273µm as shown in Figure-3.It shows that pores are inhomogeneous and spherical with narrow size distribution.
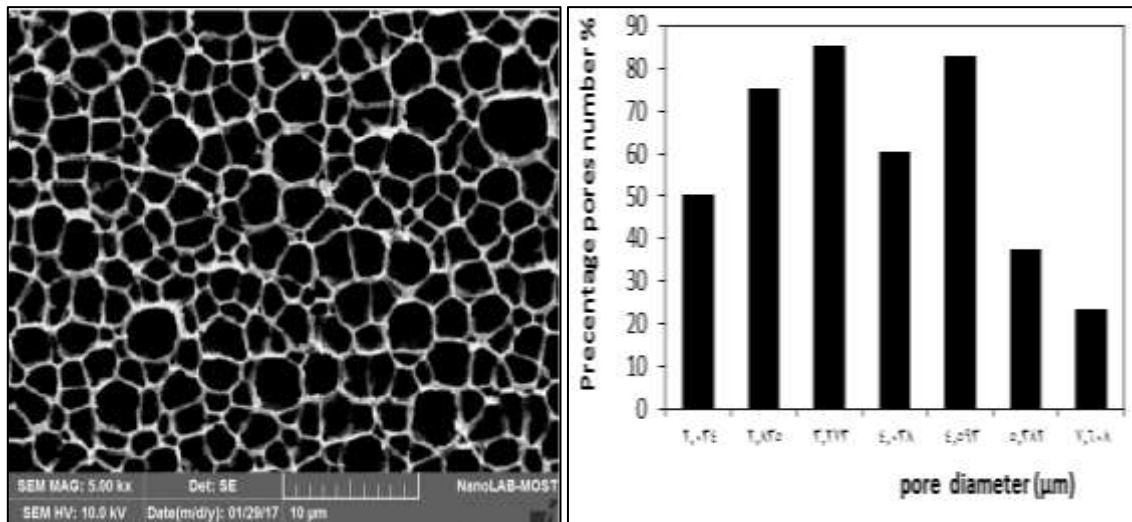
Figure 3- Illustrates the SEM image of porous layer with the statistical distribution of pores in the porous layer at etching time 5 min at laser intensity100 mW/cm^2 of about**.**

Figure-4, illustrates, the morphology of gold nanoparticles /macro-porous silicon, from this figure, it can be seen the growth the gold nanoparticles about and above pores. The reason for such fast nucleation and growing of closed pores is height value of electronegativity change between gold and silicon, and AuNPs will grow in an isotropic way depending on the amount of the (Au^{+3}) ions and the density ion reduction sites. The gold aggregation process on the porous surface was increased by increasing the aqueous solutions of $HAuCl_4$ concentration.
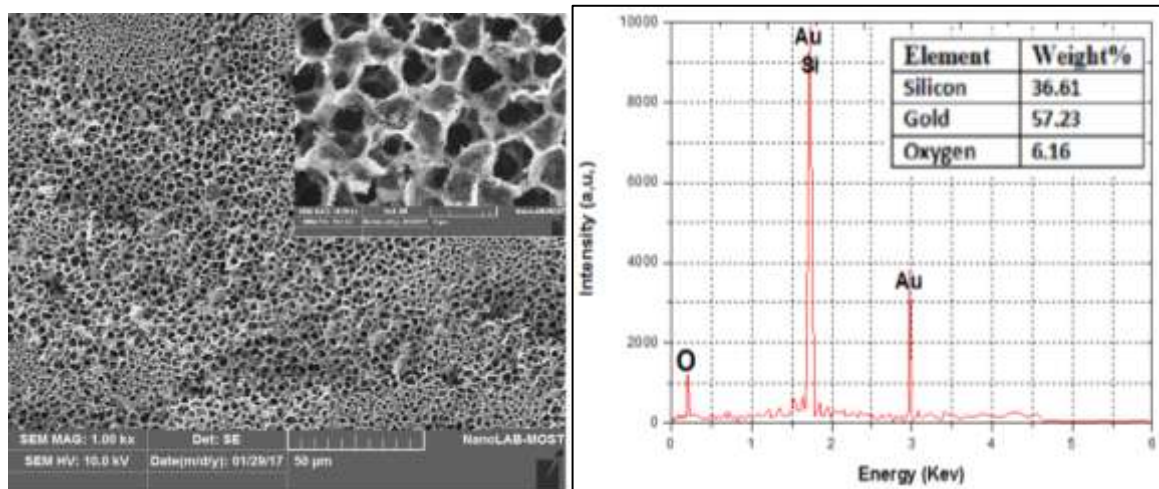
Figure 4- Illustrates the SEM image of gold nanoparticles /macro-porous silicon at etching time 5min with 10-3M and the related EDS spectra.

Figure-5 shows the diffraction pattern of the AuNPs/macroPS layer. It is presented that the PS layer stills crystalline in the plane (100) at (2θ) diffraction angle of about (32.68^o), and the values of the specific Bragg's reflections at diffraction angles of (38.3^o) and (44.16^o) for the planes (111) and (200) respectively for Au nanoparticles.
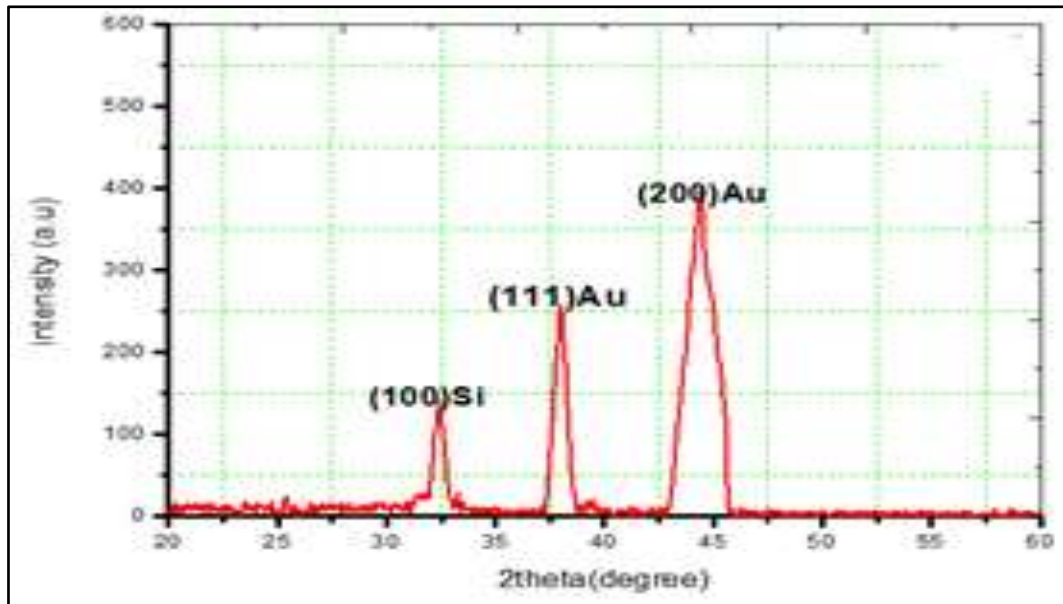
Figure 5- shows the XRD pattern of AuNPs/macroPS deposited with $HAuCl_4$ at concentrations of 10^{-3} M.

The Table-1, presents the obtained numerical results**:**

Table 1- The standards of FWHM, the size and S.S.A. of Au-NPs as a function of etching time 5min

Etching time(min)	HAuCl₄/HF concentration	Plane (111)			plane (200)		
		FWHM (rad)	Grain Size of AuNPs (nm)	S.S.A of AuNPs (m²/gm)	FWHM (rad)	Grain Size of AuNPs (nm)	S.S.A of AuNPs (m²/gm)
5 min	10^{-3}M	0.028	5	62.2	0.041	0.56	554.02

Table-1 shows that the maximum gold grain size is about(5 nm) for(10^{-3} M) of concentration at the plane (111) and the minimum gold grain size is(0.56 nm) at the plane (200), while the highest value of S.S.A. for AuNPs is about (554.02 m^2/gm) at the plane (200) and the lowest value is about (62.2 m^2/gm) in the plane(111).So, based on the obtained results of XRD analysis.

3.2. Photoluminescence (PL) spectra.

The PL spectra of bare PS samples before and after deposition process are presented in Figure-6(a). PL emission spectra of bare PS sample prepared from (100), n-type Si wafer was studied.
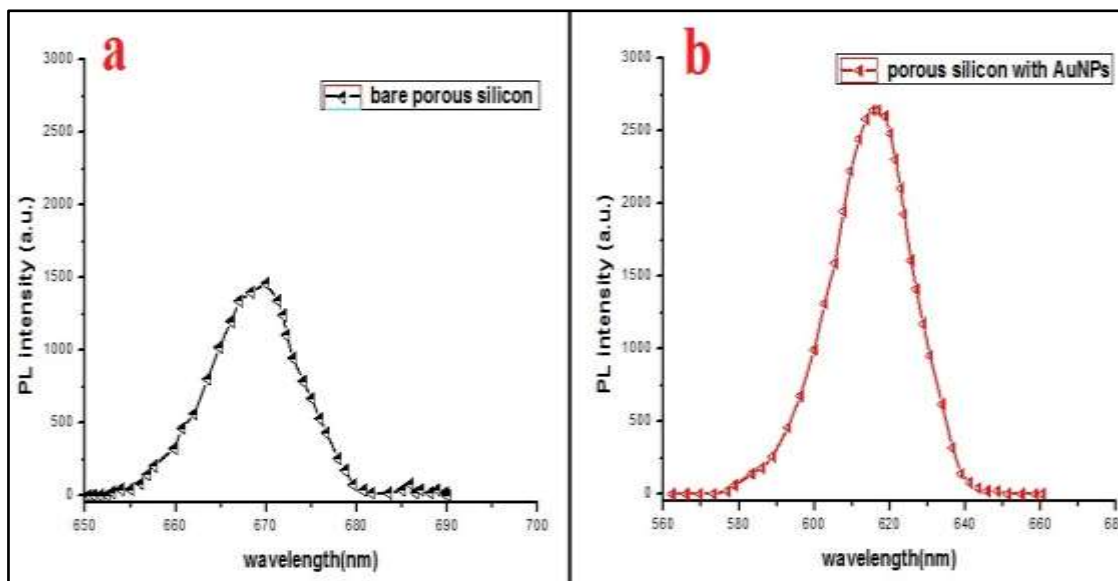
Figure 6-PL spectra of a) bare porous silicon b) porous silicon AuNPs.

The found results of PL for porosity bare structure macroPS are presented in Table-2:

Table 2- The PL emission wavelength, PS energy gap, and silicon nano-sized

Porosity(%) with time	PL wavelength(nm)	PL peak intensity (a.u)	PS energy gap(eV)	Si nano size(nm)
64	670	1460.26	1.85	3.4

The deposition of Au-NPs persuades a modification of macroPS structure and surface contents that produces either increasing or quenching of PL intensity depending on the sizes of the aggregated Au-NPs and their localities on the surface of hybrid structure macroPS as shown in Figure-6(b). The PL emission spectrum of bare macroPS was quenched to the value of (1460.26) in Figure-6(a) and then was higher in Figure-6(b) to the value of (2642.38a.u.) as compared with the Figure-6(a).

3.3.   Infrared spectroscopy (FTIR).

From Figure-7, Characterizations of chemical species on macroporous silicon surfaces were done. The FTIR signals from macro-PS were typically stronger compared with the signals obtained from the flat silicon surface due to the much larger specific area of macroPS.The hydrogen covered the dangling bonds of silicon after the etching process.Thus silane   Si-H$_x$ (x=1,2, and 3)groups were formed on the surface of the prepared porous silicon. Types of such group are governed by surface morphology. Infrared spectroscopy (FTIR) was so important and intensity of absorption bond was corresponding to the vibrational mode of H-chemical bonds.
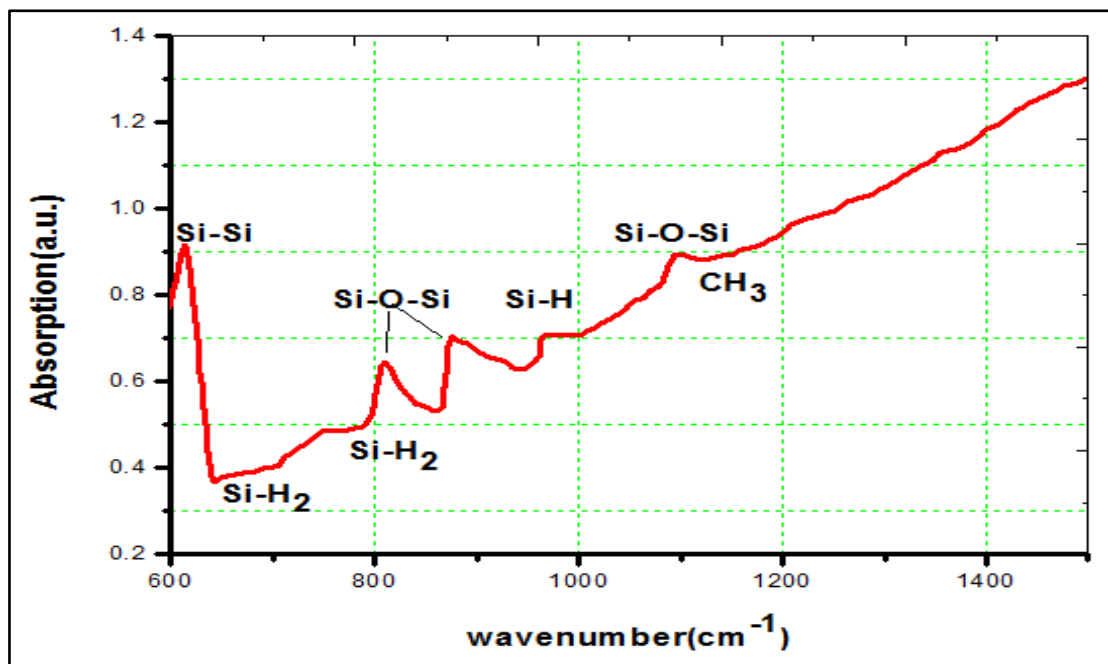
Figure 7 FTIR absorption spectra of porous silicon prepared under Ultraviolet illumination for etching time 5min.

Figure-7 illustration the FTIR absorption spectra; In this region, the spectra contain the monohydride (Si-H) bonds, dihydride (Si-H$_2$) bonds, and Si-O-Si bonds. The spectra for sample clearly presented an obvious increase in the absorption peaks related to the Si–O–Si vibration mode. This result demonstrated the great density of the silicon oxide bonds in the sample. The variation of absorption peak and wave number as a function for chemical bonds are tabulated in the Table-3.

Table 3- Wave-number positions and designations of the transmittance heights observed in several PS sample by FTIR measurements.

Highest position (cm^{-1})	Attribution
Si-Si (Bonds)	614
Si-H2 (Wagging)	642, 622
Si-H (Bending)	964
CH3 (symmetric stretching)	1116
Si-O-Si (stretching)	810,869,1094

3.4. J-V characteristics

From Figure-8 present, the J-V characteristics of Ultraviolet illuminated porous sample for the structure (Al/macroPS/n-Si/Al) at room temperature under the pressure of about 0.2mbar. For both curves, the case with gas the values of the current were higher than that of at bare macroPS the case without gas exposure CO$_2$, the J-V characteristic did not change the shape (still rectifying).The variation in the current indicating that the sensor was very sensitive to CO$_2$ gas. For both Figure-8 the variation of the current at maximum applied voltage +5V at the room temperature before and after exposure to CO$_2$ gas increased.
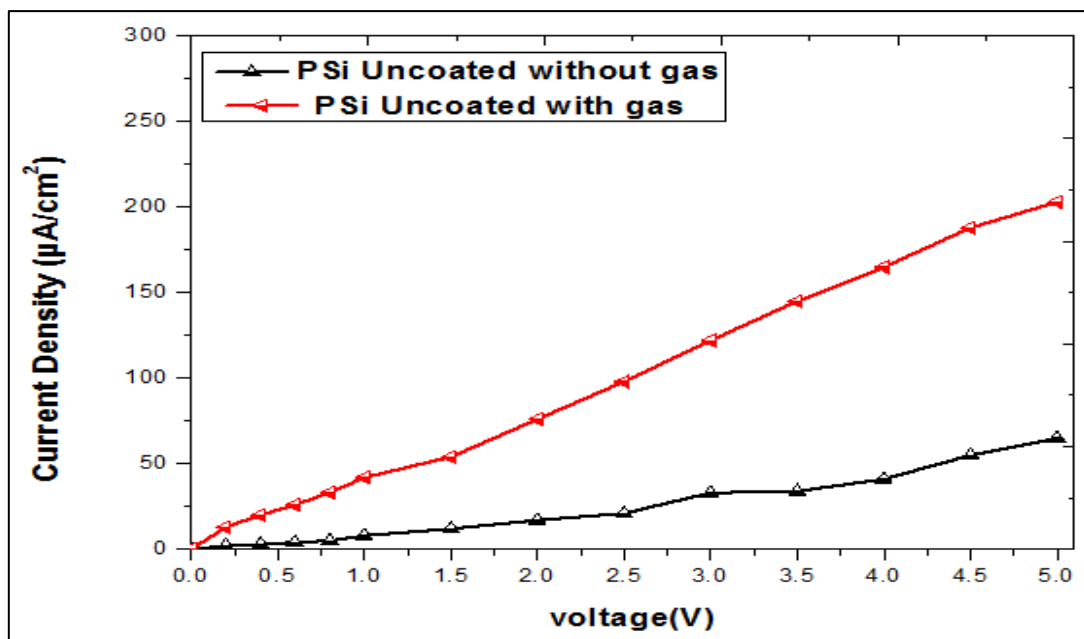
Figure 8- Current-voltage (J–V) characteristics of uncoated porous silicon with and without CO_2 gas.

In Figure-9 the presence of the AuNPs with and without the CO_2 gas would enhance the current flow in the fabricated sensor. According to the CO_2 molecules that acted as acceptor, this lead to an increase in the free carrier concentration, where the present the J-V characteristics of the porous sample, the forward current-voltage behavior as Schottky, where a rapid change in current gives a high sensitivity value at low voltage[17,22].
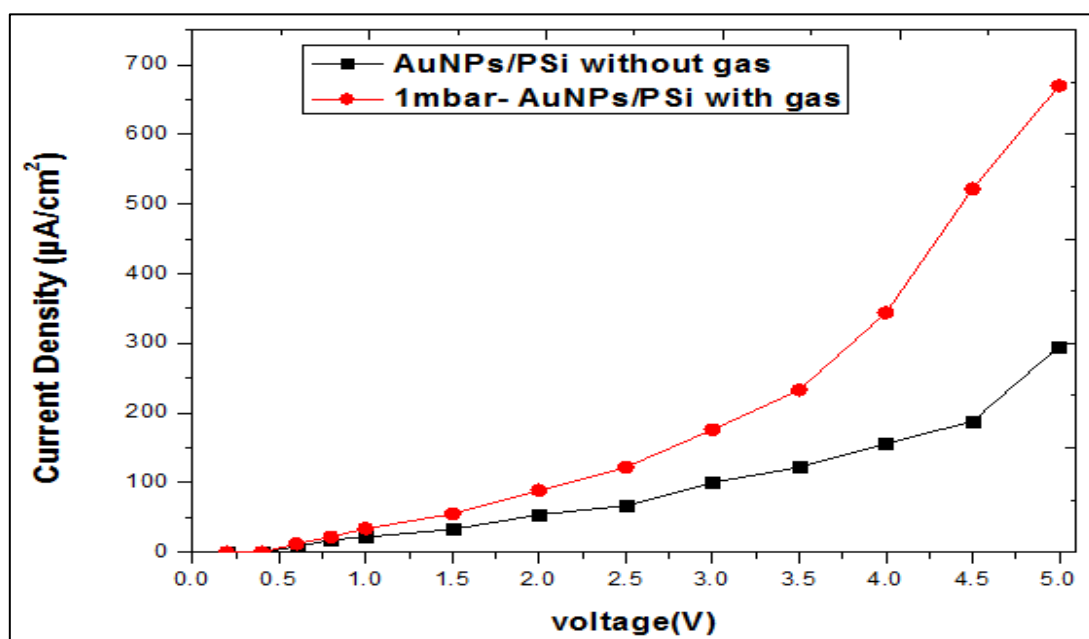
Figure 9-Current-voltage (J–V) characteristics of AuNPs on porous silicon with and without CO_2 gas.

4. Conclusions

In this research revealed the main role of the hybrid structure Au-NPs/macroPS in the CO_2 gas-sensor field owing to the phenomena of sensitivity at the silicon-gold surface. The can that Producing macro-PS layer from n-type Si wafer using photoelectrochemical etching process with a range of porosities and different pore sizes, is related to the experimental conditions and also addition solution of HAuCl4 increases the surface area efficiency resulting in adsorption of gas molecules on the surface. The gas sensing performance was connected with the structural, morphological and optical

properties of the hybrid structure macro PS and AuNPs with macroPS signify a better candidate to be employed in for sensing applications owing to their unique sensing properties.

References
1. Chen, C.H. and Chen, Y.F. **1999.** Optical properties of n-type porous silicon obtained by photoelectrochemical etching, *Solid State Communications*. **(1999)**, 681–685.
2. Seals, L., Tse, L.A., Hesketh, P.J. and Gole, J.L. **2002.** Rapid, reversible, sensitive porous silicon gas sensor, *J. Appl. Phys*. **91**: 2519–2523.
3. Gole, J.L., Seals, L.T. and Lillehei, P.T. **2000.** Patterned metallization of porous silicon from electroless solution for direct electrical contact, *J. Electrochem. Soc*. **147**: 3785–3789.
4. Jalil (Kamran) Khajehpour Tadvani. **2013.** Gold nanothorns – macroporous silicon hybrid structure: a simple and ultrasensitive platform for SERS, Ph.D. thesis, School of Applied Sciences and Engineering Faculty of Science Monash University, Australia.
5. Jawad, M.J., Hammod, H.Y. and Dheyab, A.B. **2015**. Effect of Thermal Annealing Temperatures on MSM Photo Detector Based on Ge-like Micro Flowers in the Dark Mode. *Indonesian Journal of Electrical Engineering and Computer Science*, **16**(3): 502-508.
6. Pavlikov, A.V., Lartsev, A.V., Gayduchenko, I.A. and Timoshenko, V. **2012**. Porous Silicon—*Microelectron Eng*, 90 -96.
7. Gelloz, B., Sano, H. and Boukherroub, R. **2003**. Porous Silicon—*Appl Phys Lett*, **83**: 12-2342.
8. Gabouze N, Belhousse S, Cheraga H.2006. Porous Silicon—*Vacuum*, **80**(9): 986.
9. Anderson, R.C., Muller, R.S. and Tobias, C.W. **1990**. Investigation of porous silicon for vapor sensing. *Sensors and Actuators A*, **21**: 835-39.
10. Yamazoc, N. and Shimizu, Y. **1986**. Humidity sensors: principles and applications, *Sensors and Actuators*, **10**: 379-398.
11. Kwok, W.M., Bow, Y.C., Chan, W.Y., Poon, M.C., Ran, P.G. and Wong, H. **1999**. Study of Porous Silicon Gas Sensor" (0-7803-5648-9DfV$100.1IEEE).
12. Serdar Ozdemir and James L. Gole. **2010**. Gas Transport and Response in Porous Silicon Sensors, *Mater. Res. Soc. Symp. Proc*. Vol. 1253 © Materials Research Society 1253-K05-33.
13. Bogaerts, W., de Heyn, P., van Vaerenbergh, T. **2012**. Porous Silicon— *Laser & Photonics Rev*, **6**: 1- 47.
14. Dzhafarov, T. J., Qafqaz. **2009**. Porous Silicon—*Univ*, 25- 20.
15. Ding, M., Zhao, D., Yao, B., Li, Z, Xu, X. **2015**. Ultraviolet photodetector based on heterojunction of n-ZnO microwire/p-GaN film. *RSC Adv* **5**: 908
16. Alwan, M., Alwan, Amer B. Dheyab, **2017**. Room temperature CO2 gas sensors of AuNPs/mesoPS hybrid structures' Appl Nanosci, ISSN 2190-5509.
17. Alwan M. Alwan, Intisar A. Naseef, **2017**. Optimization of photoluminescence properties of Porous silicon by adding gold nanoparticles, *Iraqi Journal of Science*, **58**(1A): 53-62.
18. Q. A. Mekeef, thesis, **2010**. Characteristics of Silicon Nanostructures Produced by High Power Laser, University of technology.
19. Diffusion Equation – Wikipedia (January **2006**) http://en.wikipedia.org /wiki/ Diffusion _ equation.
20. Herrn, J., Mandayo, G.G., Castano, E. **2008**. Solid state gas sensor for fast carbon dioxide detection, Sens. *Actuators B*, **129**: 705–709.
21. Ismail, R.A., Alwan, A.M., Ahmed, A.S. **2017**. Preparation and characteristics study of nano-porous silicon UV photodetector, Journal springer, *Appl Nanosci Appl Nanosci*, **7**: 9–15.
22. Alwan, M., Abbas, R.A. **2017**. EFFECTS OF THE POROUS SILICON MORPHOLOGY ON THE GAS SENSOR PERFORMANCE, *International Journal of Engineering Sciences & Research Technology*, **6**(1): 204-217.